Multizone Navier–Stokes Computations for a Transonic Projectile using MacCormack Finite Difference Method

Tzu–Chang Chen
Graduate Student of Power Mechanical Engineering
Ching–Chang Chieng
Professor of Nuclear Engineering
National Tsing Hua University
Hsinchu, Taiwan
Republic of China

Abstract

MacCormack's explicit and unsplit method is employed on a multizone overlap grid–system to predict the transonic, turbulent flowfield around an axisymmetric projectile at zero angle of attack. The computational results compared with wind tunnel measurements of boundary layer surveys are performed. Two different grid systems, depending on how the projectile base is modeled: (1) the projectile with the flat base as the actual projectile. (2) the projectile with the extended boattail as a simplified model. The computational results show that the agreement with experiment can be obtained and convergence is significantly improved if the locally varying time step proposed by Kunz(1991) is employed.

Nomenclature

Equation Symbols:

x,y	axial and normal cartesian coordinates
Q'	variables vector in cartesian coordinates
E', F'	flux vector in x, y direction
ξ, η	transformed coordinates
Q	variables vector in transformed coordinates
E, F	flux vector in ξ, η direction
B_i, C_j D_i	coefficient terms in Navier–Stokes equation
S_1, S_2 T_1, T_2	viscous terms in Navier–Stokes equation
G_1, G_2	axisymmetric viscous terms in Navier–Stokes equation
H	source term in Navier–Stokes equation
J	Jacobian

Fluid Properties:

ρ	density (lb/ft^3)
u, v	axial velocity, normal velocity (ft/sec)
U, V	contraviant velocity (sec^{-1})
t	time (sec)
p	pressure (lbf/ft^2)
T	temperature (R)
e	unit energy (ft^2/sec^2)
R	gas constant (1716 ft^2/sec^2·R)
μ, μ_t	laminar and turbulent viscosity coefficients (lb·sec/ft^2)
Pr,Pr_t	laminar and turbulent Prandtl number
Cv	specific heat of constant volume (4290ft^2/sec^2·R)
Cp	specific heat of constant pressure (6006ft^2/sec^2·R)
C_P	pressure coefficient
k	conductivity coefficient
M	Mach number
Re	Reynolds number
D	diameter of SCOBT projectile

Subscript:

i, j	grid indice
∞	freestream value

I. Introduction

A projectile in flight will experience some critical aerodynamic behavior in the regime of transonic speed, which is the range between M_∞=0.9 and 1.1. In this range of speed, the aerodynamic coefficients change abruptly. The complexity of shock structure is formed on body which causes such a flow phenomenon. The flowfield is characterized by the strong viscous–inviscid interaction, shock–boundary layer interaction and the separation near the projectile base.

Most of early researches about transonic projectile flowfield were based on small disturbance potential theory. Krupp & Murman[1](1972) and Chow, et al[2](1975) provided qualitative predictions of transonic projectile by application of this theory. Because potential theory doesn't consider the effects of viscosity, recent researches tend to deal with the flowfield by thin layer Navier–Stokes equation. Most famous and widely used numerical schemes are Beam and Warming, Flux–Splitting and TVD schemes.., etc. For example, Deiwert[3] studied the 3–D boattail afterbody flow field by applying Beam & Warming[4]. Sahu & Danberg[5,6] solved the flowfields about the modified projectile with extended boattail by using the same method and the flux–splitting scheme. Hsu[7] employed the TVD scheme to study the same problem.

Present work will solve the full Navier–Stokes equations instead of thin–layer type equations by using the MacCormack explicit[8] scheme. In addition, an overlap multizone technique is used for the grid–system generation so that better resolution and easier grid generation can be obtained. This study is extended from the work developed by Patel and Sturek[9]. However, a locally varying time step proposed by Kunz[11] in 1991 is employed to satisfy the crucial criteria for this explicit scheme. Due to the improvement of convergence, application of this time step evidently increases the efficiency of MacCormack explicit scheme without adding any artificial dissipation term.

II. Numerical Treatment

Governing Equations

The mean flow is described by two–dimensional mass, momentum and energy conservation equations, which are full time dependent, mass averaged Navier–Stokes equations. The dimensional governing equations in generalized curvilineaar coordinates are represented as follows,

$$\frac{\partial Q}{\partial t}+\frac{\partial E}{\partial \xi}+\frac{\partial F}{\partial \eta}+\frac{1}{J\cdot y}\cdot(F'+H')\beta \qquad (2.1)$$
$$= \frac{\partial}{\partial \xi}S_1(Q,Q_\xi)+\frac{\partial}{\partial \xi}S_2(Q,Q_\eta)+\beta\frac{\partial}{\partial \xi}G_1$$
$$+ \frac{\partial}{\partial \eta}T_1(Q,Q_\xi)+\frac{\partial}{\partial \eta}T_2(Q,Q_\eta)+\beta\frac{\partial}{\partial \eta}G_2$$

where

$$Q = \frac{1}{J}\begin{bmatrix}\rho\\ \rho u\\ \rho v\\ \rho e\end{bmatrix} \qquad (2.2)$$

$$E=\frac{1}{J}\begin{bmatrix}\rho U\\ \rho uU+\xi_x p\\ \rho vU+\xi_y p\\ (\rho e+p)U\end{bmatrix} \qquad F=\frac{1}{J}\begin{bmatrix}\rho V\\ \rho uV+\eta_x p\\ \rho vV+\eta_y p\\ (\rho e+p)V\end{bmatrix}$$

$$S_1=\frac{1}{J}\begin{bmatrix}0\\ B_1u_\xi + B_2v_\xi\\ B_2u_\xi + B_3v_\xi\\ B_1uu_\xi + B_2(vu_\xi+uv_\xi)+B_3vv_\xi+B_4T_\xi\end{bmatrix}$$

$$S_2=\frac{1}{J}\begin{bmatrix}0\\ C_1u_\eta + C_2v_\eta\\ C_3u_\eta + C_4v_\eta\\ C_1uu_\eta + C_2uv_\eta+C_3vu_\eta+C_4vv_\eta+C_5T_\eta\end{bmatrix}$$

$$T_1=\frac{1}{J}\begin{bmatrix}0\\ C_1u_\xi + C_3v_\xi\\ C_2u_\xi + C_4v_\xi\\ C_1uu_\xi + C_2vu_\xi+C_3uv_\xi+C_4vv_\xi+C_5T_\xi\end{bmatrix}$$

$$T_2=\frac{1}{J}\begin{bmatrix}0\\ D_1u_\eta + D_2v_\eta\\ D_2u_\eta + D_3v_\eta\\ D_1uu_\eta + D_2(vu_\eta+uv_\eta)+D_3vv_\eta+D_4T_\eta\end{bmatrix}$$

$$G_1=\frac{1}{J}(\mu+\mu_t)\begin{bmatrix}0\\ -2/3\xi_x(v/y)\\ -2/3\xi_y(v/y)\\ -2/3\xi_x(v/y)u-2/3(\mu+\epsilon)\xi_y(v^2/y)\end{bmatrix}$$

$$G_2=\frac{1}{J}(\mu+\mu_t)\begin{bmatrix}0\\ -2/3\eta_x(v/y)\\ -2/3\eta_y(v/y)\\ -2/3\eta_x(v/y)u-2/3(\mu+\epsilon)\eta_y(v^2/y)\end{bmatrix}$$

$\beta = \begin{cases}1 & \text{for axisymmetric case.}\\ 0 & \text{for 2-D case.}\end{cases}$

$J = \xi_x\eta_y - \xi_y\eta_x$

$U = \xi_x u - \xi_y v$

$V = \eta_x u - \eta_y v$

Where S_1, S_2, T_1, T_2 are viscous terms, the coefficients B_i, C_j, D_i are defined as follows:

$$B_1 = (\mu+\mu_t)(\xi_y^2 + 4/3\ \xi_x^2) \qquad (2.3)$$
$$B_2 = (\mu+\mu_t)(1/3\ \xi_x\xi_y)$$
$$B_3 = (\mu+\mu_t)(\xi_x^2 + 4/3\ \xi_y^2)$$
$$B_4 = \frac{1}{\gamma-1}\left(\frac{\mu}{P_r}+\frac{\mu_t}{P_{rt}}\right)(\xi_x^2+\xi_y^2)$$
$$C_1 = (\mu+\mu_t)(\xi_y\eta_y + 4/3\ \xi_x\eta_x)$$
$$C_2 = (\mu+\mu_t)(\xi_y\eta_x - 2/3\ \xi_y\eta_x)$$
$$C_3 = (\mu+\mu_t)(\xi_x\eta_y - 2/3\ \xi_y\eta_x)$$
$$C_4 = (\mu+\mu_t)(\xi_x\eta_x + 4/3\ \xi_y\eta_y)$$
$$C_5 = C_P\left(\frac{\mu}{P_r}+\frac{\mu_t}{P_{rt}}\right)(\xi_x\eta_y + \xi_y\eta_y)$$
$$D_1 = (\mu+\mu_t)(\eta_y^2 + 4/3\ \eta_x^2)$$
$$D_2 = (\mu+\mu_t)(1/3\ \eta_x\eta_y)$$
$$D_3 = (\mu+\mu_t)(\eta_x^2 + 4/3\ \eta_y^2)$$
$$D_4 = C_P\left(\frac{\mu}{P_r}+\frac{\mu_t}{P_{rt}}\right)(\eta_x^2+\eta_y^2).$$

The axisymmetric source terms (F'+H') can be expressed as follows, i.e.

$$(F'+H')=\begin{bmatrix}\rho v & -AV_{11}-AV_{21}\\ \rho uv & -AV_{12}-AV_{22}\\ \rho vv & -AV_{13}-AV_{23}\\ (\rho e+p)v & -AV_{14}-AV_{24}\end{bmatrix} \qquad (2.4)$$

where AV_{ij} (i = 1,2 and j = 1,2,3,4) are defined as follows:

$$AV_{11} = 0.0 \qquad (2.5)$$
$$AV_{12} = (\mu+\mu_t)(\xi_y u_\xi + \xi_x v_\xi)$$
$$AV_{13} = 2(\mu+\mu_t)(\xi_y v_\xi)$$
$$AV_{14} = C_P\left(\frac{\mu}{P_r}+\frac{\mu_t}{P_{rt}}\right)\xi_y T_\xi + (\mu+\mu_t)(4/3\xi_y vv_\xi - 2/3\xi_x vu_\xi) + (\mu+\mu_t)(\xi_y uu_\xi + \xi_x uv_\xi)$$
$$AV_{21} = 0.0$$
$$AV_{22} = (\mu+\mu_t)(\eta_y u_\eta + \eta_x v_\eta)$$
$$AV_{23} = 2(\mu+\mu_t)(\eta_y v_\eta - v/y)$$
$$AV_{24} = C_P\left(\frac{\mu}{P_r}+\frac{\mu_t}{P_{rt}}\right)\eta_y T_\eta + (\mu+\mu_t)(4/3\eta_y vv_\eta - 2/3\eta_x vu_\eta - 2/3v^2/y) + (\mu+\mu_t)(\eta_y uu_\eta + \eta_x uv_\eta)$$

Turbulence Model

In this article, the mixing-length turbulence model proposed by Baldwin and Lomax[12] is used to compute the turbulent viscosity, i.e.

$$\mu_t = \begin{cases}(\mu_t)_{inner} = \rho\ell^2\ |\ w\ |, & y \le y_{crossover}\\ (\mu_t)_{outer} = kC_{CP}\ \rho\ F_{wake}F_{kleb}(y), & y > y_{crossover}\end{cases} \qquad (2.6)$$

where, y is the normal distance from wall. $y_{crossover}$ is the minimum y for $(\mu_t)_{inner} = (\mu_t)_{outer}$.

Numerical Procedure

The MacCormack's explicit method is employed for solving the governing equations. The predictor-corrector steps are

Predictor:

$$Q_{i,j}^{\overline{n+1}} = Q_{i,j}^{n} - \Delta t(E_{i,j}^{n} - E_{i-1,j}^{n}) - \Delta t(F_{i,j}^{n} - F_{i,j-1}) \qquad (2.7)$$

Corrector:

$$Q_{i,j} = \frac{1}{2}[Q_{i,j}^{n} + Q_{i,j}^{\overline{n+1}} - \Delta t(E_{i+1,j}^{\overline{n+1}} - E_{i,j}^{\overline{n+1}}) - \Delta t(F_{i,j+1}^{\overline{n+1}} - F_{i,j}^{\overline{n+1}})] \qquad (2.8)$$

Where $E_{i,j}^{\overline{n+1}}$ implies that the terms are evaluated using $Q_{i,j}^{\overline{n+1}}$ and so forth. This explicit scheme is 2nd order accurate in time and space. Also because of its simplicity in solving equations, the program can be easily vectorized. However, for the explicit method the timestep size must not exceed the maximum by the CFL condition. An approximate linearized stability analysis for the inviscid equations yields the following inviscid time step:

$$\Delta t = \frac{1}{\frac{|U|}{\Delta\xi}+\frac{|V|}{\Delta\eta}+a\left\{\left(\frac{\xi_x}{\Delta\xi}+\frac{\eta_x}{\Delta\eta}\right)^2+\left(\frac{\xi_y}{\Delta\xi}+\frac{\eta_y}{\Delta\eta}\right)^2\right\}^{\frac{1}{2}}} \qquad (2.9)$$

where a is the speed of sound.

The equation (2.9) was usually multiplied by a factor (denoted as CFL) that is smaller than one. Ths choice of Δt affects the rate of convergence tremendously and will be discussed in the next section.

Local Time Step

In order to increase the convergency rate of the numerical computation, different varying timesteps are proposed by many investigators, such as space varying Δt[10] in Beam–Warming scheme. Present work will employ a locally varying timestep proposed by Kunz[11]. This time step is derived from the linear stability analysis of Navier–Stokes equation, which is more complete than the conventional local time step. Its form is:

$$\Delta t = \mathrm{Min}\,[\,\Delta t_c\,,\,\Delta t_v\,] = \mathrm{Min}\,\left[\frac{\mathrm{IMAG}}{|U|+a\sqrt{\nabla\xi\nabla\xi}+|V|+a\sqrt{\nabla\eta\nabla\eta}}\,,\ \frac{\mathrm{REAL}}{\frac{4\gamma}{\rho}\left(\frac{\mu}{P_r}+\frac{\mu_t}{P_{rt}}\right)\left[(\nabla\xi\nabla\xi)+(\nabla\eta\nabla\eta)\right]+\frac{4}{3\rho}(\mu+\mu_t)}{\left[7(\nabla\xi\nabla\xi)+\sqrt{(\nabla\xi\nabla\xi)(\nabla\eta\nabla\eta)}\right]}\right] \qquad (2.10)$$

where IMAG and REAL are input parameters corresponding to operational CFL number and Von Neumann number respectively. Both values are restricted to be less than 1 in order to ensure numerical steady. In (2.10), Δt_c comes from hyperbolic consideration, which corresponds to convection effect and have the same form as the conventional time step. Δt_v is obtained from parabolic consideration, which includes the correspondence effects of viscosity and grids system.

Grids system

In order to perform the computation, the multizone approach is employed to get grid–system. The major advantages of this method are: (1) individual subgrid can be achieved by simple spacing technique and get good resolution. (2) subgrids can be easily calculated by parallel computing. (3) it's convenient in adding dense grids over flowfield of large gradient. (4) suitable for large computation on machine of smaller memory.

In the calcuation of transonic projectile, the first grid spacing normal to the wall are required to be fine enough so that the y^+ can be controlled at less than 5. It implies that the first Δy is set to be 0.00002D and the entire turbulent boundary layer can be obtained. H grids are adopted here for simplicity. Different subgrid boundaries are connected by the same grid distribution, and to be the boundary condition of each other in next iteration.

Results and Discussions

Generations of the Grid Systems

The turbulent flow fields past a secant–ogive–cylinder–boattail(SCOBT) projectile(Fig.1) at zero angle of attack at freestream Mach number of 0.94 and 0.97 are computed for the present study. Surface pressure distribution is predicted to compare with measurement.

The computation is performed on two grid–systems:
(A) Projectile with extended boattail: The flow field around the flat base of SCOBT projectile is approximately predicted by the extended projectile. This projectile is extended from the cylinder base to 2.52D afterward by a circular cone of 7.64°, where the diameter of cone is 0.2D.

This grid system is composed of two subgrids, which is shown in Fig.2. The two grids are (1)31x75 grid points to cover the freestream region, and (2)106x50 grid points around the projectile. The range of computation domain are: 10D from the nose of the projectile to freestream boundary, 14D from no reflection boundary to the projectile surface, 12D downstream the nose.

(B) Projectile with flat base: This is the real geometry of the projectile and three subgrid–systems covers the computational domain. The grid points of these subsystems are (1)31x75, (2)111x51, (3)45x31 (Fig.3). The subgrid systems 1 and 2 are generated the same as those for the extended projectile. Subgrid–system 3 covers the base flow region. Distance of 6.2D downstream the base corner to the outer boundary is chosen. The grid resolution is highly dense near the base corner in order to predict the corner expansion. Because of the abrupt change near the corner, the computational result by this grid system is more difficult to be obtained than that by the former grid–system.

Surface Pressure

The computed pressure coefficients along the projectile for Mach numbers of 0.94 and 0.97 are compared with the experimental data[13,14] and shown in Fig.4 and Fig.5 respectively. For the case of Mach number 0.94, the calculated value is consistent with the experiment even near the shock. The expansion is majorly due to the change of projectile curvature, and the shock is formed because of acceleration of fluid and the back pressure. Same degree of accuracy is obtained by the different grid–system with the extended boattail and with the flat base. In the case of Mach number 0.97, similar result is observed. The only difference caused by the different Mach numbers is the shift of shock wave location. This phenomenon can be seen in the Mach contours also. In Figures 6 and 7, the mach number contours are illustrated by the range from M_∞=0 to M_∞=1.2.

Iteration History

The convergence criteria of explicit schemes is always crucial. It's not easy to control especially in the flowfield of highly stretched grid system, strong viscous effect and critical phenomena. There coexists the strong viscous–inviscid interaction, shock–boundary layer interaction and separation flow near projectile base, the critical phenomena are more evident. In order to obtain better convergence, Kunz's locally varying time step is adopted here instead of the conventional inviscid time step. Figure 8 plots the iteration history in the case of projectile with extended boattail at Mach number of 0.94 if conventional inviscid time step is employed. The residuals are difficult to be reduced to an acceptable level even after 20,000 iterations in the region of subgrid2. The residual for the subgrid 1 of free stream region is raised to a constant level after an order of magnitude drop. Inviscid CFL is chosen as 0.5 in the computation. Therefore, it is difficult to accept the computed results by employing this conventional inviscid time–step.

When the Kunz's local time step is applied, the constants in eq(2.10) are chosen as REAL=0.1, IMAG=0.9. The term Δt_v considers both the influences of grid–resolution and viscosity. During the computation, 3.6% of subgrid 1 and 41.57% of subgrid 2 employing Δt_v, and the rest employing Δt_c(which is the inviscid time step) as the time step. Figure 9 indicates that residuals in two subgrid–systems are efficiently lowered continuously. It is also noted that the time step of IMAG=0.9 is larger than inviscid CFL=0.5. It means that the larger local time step is taken in the inviscid region of uniform grid spacing, but a smaller time step(REAL=0.1) is chosen in the region of greater $\Delta\eta$ and viscosity. The comparison of Fig.8 and 9 implies that employing Kunz's local time step is superior to conventional time step for the case of projectile with extended boattail.

Figure 10 plots the iteration history for the case of projectile with flat base if conventional inviscid time step of CFL=0.5 is applied. Same characteristics are observed for two subgrids(grid 1,grid 2) as those for the two subgrids in Fig.8. The residuals for the third subgrid(grid

3) of base region continuously oscillate severly because of the complexity of recirculation flowfield. If Kunz's local time step of REAL=0.05 and IMAG=0.7 is applied, the percentage of the Δt_v used in respective subgrids 1,2 and 3 are: 7.43%, 29.2%, 87%. The convergence is significantly improved by employing the Kunz's local time step(Fig.11). This figure shows that (1) the oscillation of grid1 is eliminated, (2) the convergency is improved for the subgrid 2, (3) convergence characteristics for subgrid3 of base region is greatly improved and is different from the former iteration histories of all others.

Conclusion

The application of the explicit scheme of MacCormack is successfully adopted for the computation of the turbulent transonic flow past projectiles with extended boattail or flat base, if the locally varying time step of Kunz is adopted. The convergence is difficult to judge if the convemtional inviscid time step is applied and the residuals can not be reduced to an acceptable level. The convergence can be achieved and greatly improved if the Kunz's local time step is used. The use of local time step leads the possibility of employing explicit scheme for solving Navier–Stokes equation.

References

1. Krupp, J.A. and Murman, E.M., "Computational Transonic Flows Past Lifting Airfoils and Slender Bodies," AIAA Journal Vol. 10, July 1972, pp.880,886.
2. Chow, W.L., Bober, L.J. and Anderson, B.H., "Numerical Calculation of Transonic Boattail Flow," NASA TN D–7984, June 1975.
3. Deiwert, G.S., "Numerical Simulation of Three–Dimensional Boattail Afterbody Flowfields," AIAA Journal Vol. 19, No.5, May 1981, pp.582–588.
4. Beam, R. and Warming, R.F. "An Implicit Factored Scheme for Compressible Navier–Stokes Equations," AIAA Paper No.77–645, June 1977.
5. Sahu, J and Danberg, J.E., "Navier–Stokes Computations of Transonic Flows with a Two–Equation Turbulence Model," AIAA Journal Vol.24, No.11, November 1986, pp.1744–1751.
6. Sahu, J., "Numerical Computations of Transonic Critical Aerodynamic Behavior," AIAA Paper No.88–4038–CP.
7. Hsu, C.C., Shiau, N.H. and Reed, C.W., "Numerical Simulation of Transonic Turbulent Flow Past a Real Projectile," AIAA Paper No.88–0218, January 11–14, 1988.
8. MacCormack, R.W. "The Effect of Viscosity in Hypervelocity Impact Cratering." AIAA Paper 69–354, Cincinnati, Ohio.
9. Patel, N. and Sturek, R., "Parallel Numerical Simulations of Axisymmetric Projectile Flows Using Zonal–overlapped Grids", BRL–MR–3834, Ballistic Research Labortary, Aberdeen Proving Ground, Maryland, U.S.A., May, 1990.
10. Sahu, J. and Nietubicz, C. "Improved Numerical Prediction of Transonic Flow", BRL–TR–2784, Ballistic Research Labortary, Aberdeen Proving Ground, Maryland, U.S.A., March 1987.
11. Kunz, R.F., Lakshminarayana, B., "Stability of Explicit 3D Navier–Stokes / k–ϵ Procedures in Complex Internal Flow Calculations," AIAA Paper No.91–0018, Jan 7–10, 1991 / Reno, Navada.
12. Baldwin, B.S. and Lomax, H., "Thin Layer Approximation and Algebraic Model for Separated Turbulent Flows," AIAA Paper No.78–257, January 1978.
13. Chieng, C.C. and Danberg,J. "Transonic Navier–Stokes Computations for a Projectile at Angle of attack and Comparison with experiment", BRL–TR–2960, Ballistic Research Labortory, Aberdeen proving Ground, Maryland, December 1988..
14. Miller, M.C. and Molnar, J.W., "Wind Tunnel Measurements of the Induced Surface Pressure on a Spinning Artillery Projectile Model in the Transonic Speed Regime," Chemical Research, Development and Engineering Center, CRDEC–TR–86081, Sept 1986.

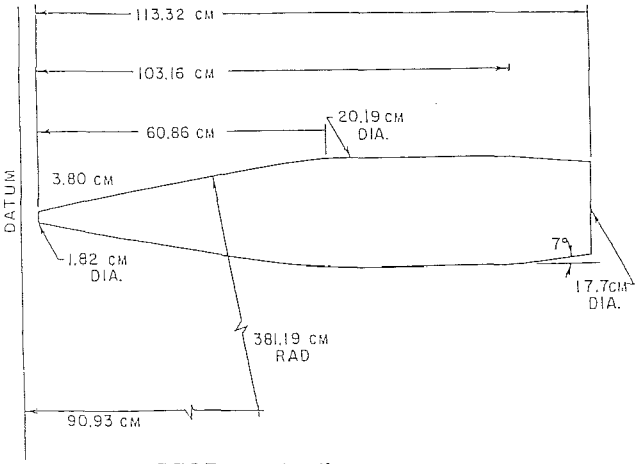

Figure 1 SCOBT projectile.

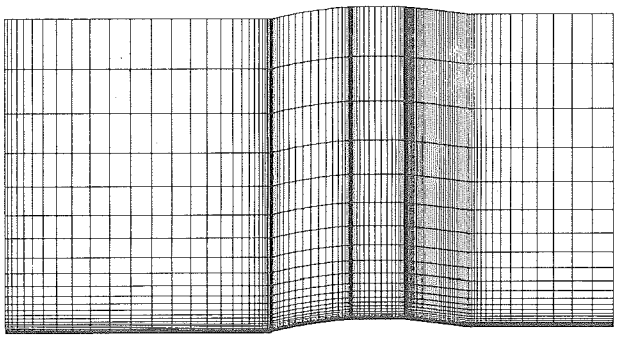

Figure 2 Grids system of extended SCOBT projectile.

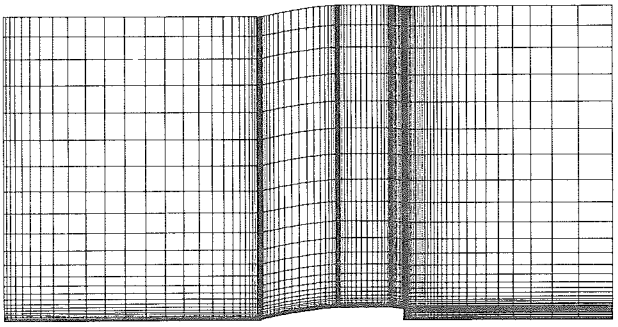

Figure 3 Grids system of flat base SCOBT projectile.

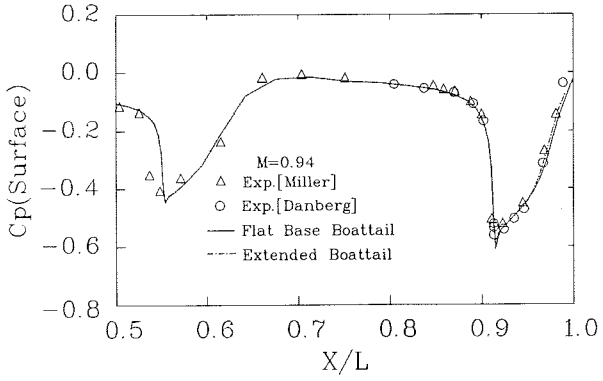

Figure 4 Surface pressure coefficient at M_∞=0.94.

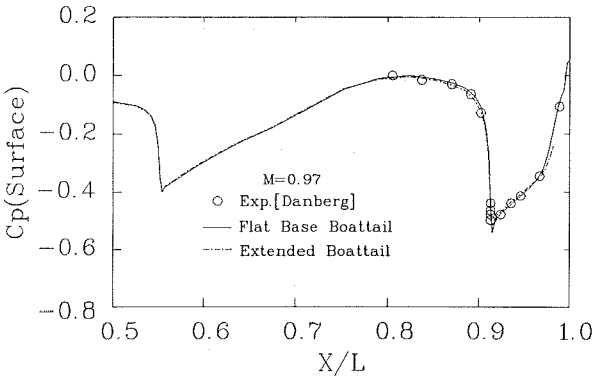

Figure 5 Surface pressure coefficient at M_∞=0.97.

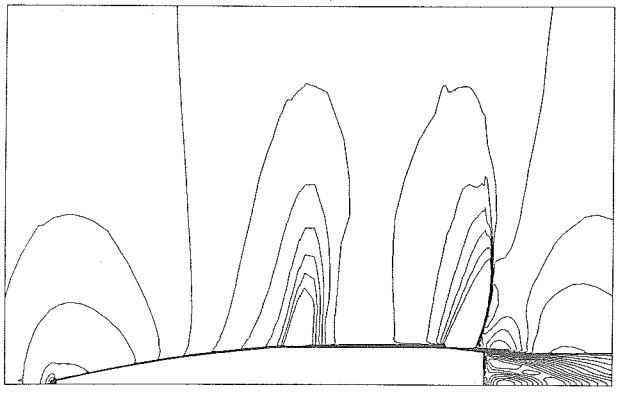

Figure 6 Mach number contour for projectile with flat base at M_∞=0.94.

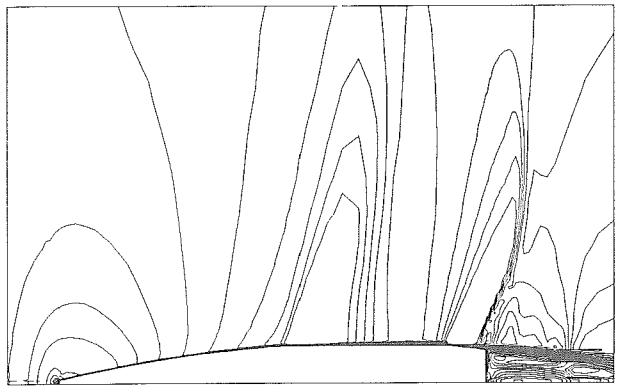

Figure 7 Mach number contour for projectile with flat base at M_∞=0.97.

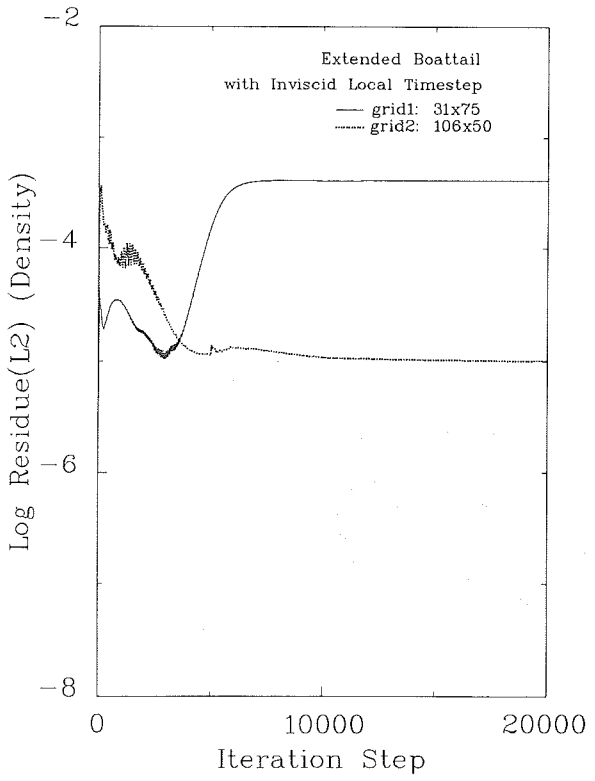

Figure 8 Iteration history for projectile with extended boattail using inviscid local time step at M_∞=0.94.

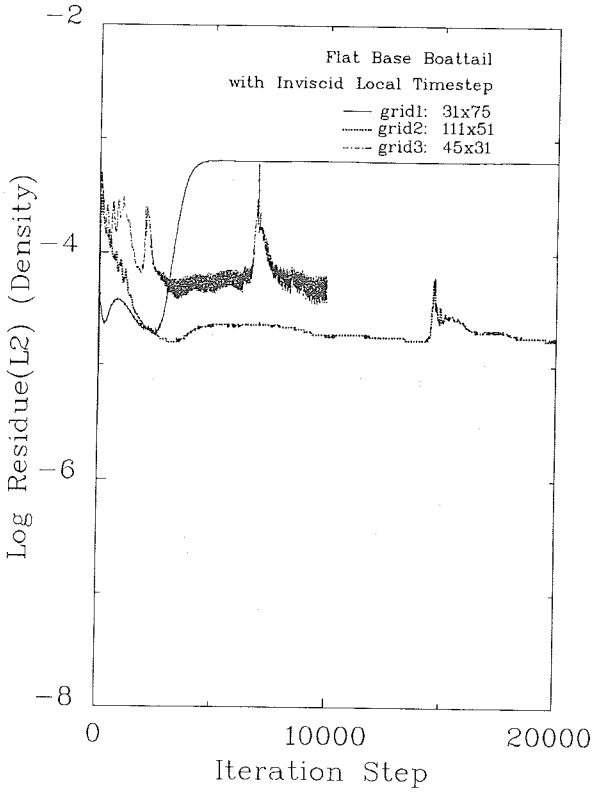

Figure 10 Iteration history for projectile with flat base using inviscid local time step at M_∞=0.94.

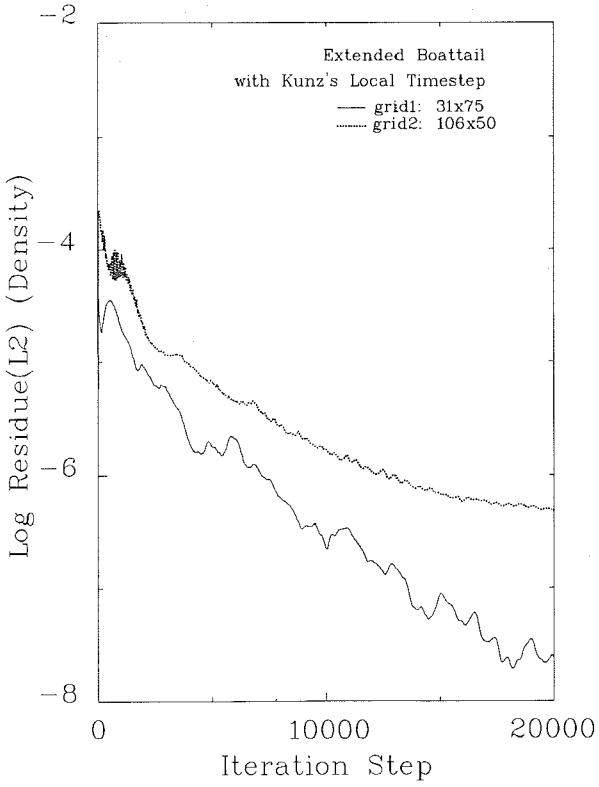

Figure 9 Iteration history for projectile with extended boattail using Kunz's local time step at M_∞=0.94.

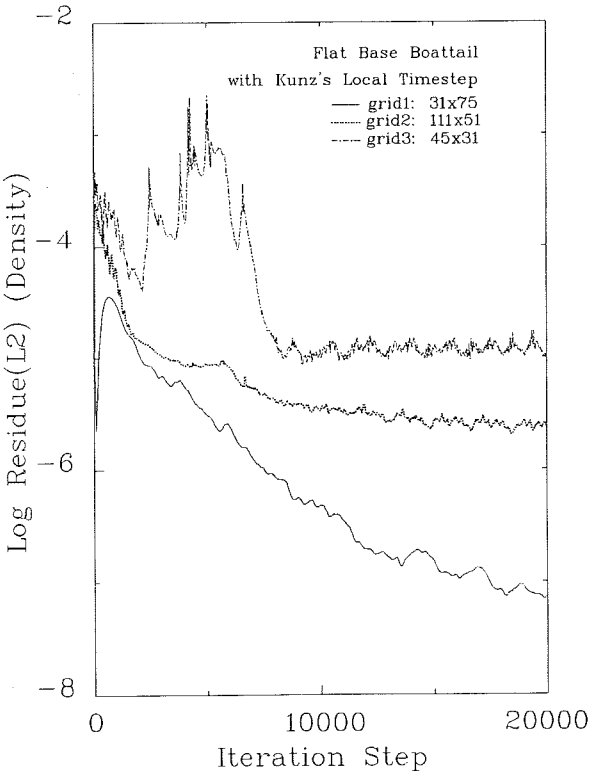

Figure 11 Iteration history for projectile with flat base using Kunz's local time step at M_∞=0.94.